

# 异质 a-C:H/a-C:H:F 配副的摩擦学行为研究

唐诗琪<sup>1</sup>, 邢朝阳<sup>2</sup>, 王圆圆<sup>2</sup>, 张俊彦<sup>2</sup>, 张斌<sup>1,2\*</sup>

(1. 许昌学院, 河南 许昌 461002; 2. 中国科学院兰州化学物理研究所先进润滑与防护材料研究发展中心, 兰州 730000)

**摘要:** 目的 研究 F 元素掺杂非晶碳基薄膜与 a-C:H 薄膜摩擦配副的摩擦学行为机制。方法 利用 PECVD 法在 Si 基底上制备 a-C:H:F 薄膜, 与直径为 6.0 mm 的 a-C:H 薄膜摩擦对偶球组成摩擦配副体系, 使用往复模式的 CSM TRB 3 摩擦机研究 a-C:H:F 薄膜的摩擦学特性, 频率为 5 Hz, 滑动总次数为 9 000, 外加载荷分别为 2、4、6、8、10 N。通过纳米硬度、X 射线光电子能谱、傅里叶红外光谱、激光共聚焦拉曼光谱、场发射扫描电镜及 CSM 摩擦试验机等, 分别评价 a-C:H:F 薄膜的结构、表面形貌、力学性能、摩擦学性能等。结果 在干摩擦环境下, 随着载荷的增加, a-C:H:F 薄膜的摩擦因数逐渐降低, 平稳后摩擦因数低至 0.018。通过掺杂 F 元素, 一方面促进了薄膜的  $sp^2$ -C 杂化, 另一方面增大了薄膜的无序度。F 元素具有钝化薄膜表面和静电排斥的作用, 使得 a-C:H:F 薄膜具有较低的摩擦因数和磨损率。结论 采用 PECVD 方法制备的 a-C:H:F 薄膜具有更好的减摩降损能力。

**关键词:** 摩擦学性能; F 元素掺杂改性; 类金刚石薄膜; 等离子体增强化学气相沉积

**中图分类号:** TH117   **文献标志码:** A   **文章编号:** 1001-3660(2024)07-0107-09

**DOI:** 10.16490/j.cnki.issn.1001-3660.2024.07.011

## Tribological Properties of a-C:H Sliding on a-C:H:F Films

TANG Shiqi<sup>1</sup>, XING Zhaoyang<sup>2</sup>, WANG Yuanyuan<sup>2</sup>, ZHANG Junyan<sup>2</sup>, ZHANG Bin<sup>1,2\*</sup>

(1. Xuchang University, Henan Xuchang 461002, China; 2. Research and Development Center for Advanced Lubrication and Protective Materials, Lanzhou Institute of Chemical Physics, Chinese Academy of Sciences, Lanzhou 730000, China)

**ABSTRACT:** Reducing friction not only promotes the life and safety of the mechanical part, but also saves energy by lowering the friction force. Many films, like carbide, nitride and boride films, have been employed to reduce friction for moving parts. Among them, carbon based films have been thought to be the best choice due to their low friction, high anti-wear and high anti-corrosion properties, etc. However, these films are combined with  $sp^2$  and  $sp^3$  bonding structures and sometimes they are doped with hydrogen (H) or fluorine (F) or other elements, such as Si, P, Ti, Cr, etc. However, since H and F have single electrons that can terminate on the dangling  $\sigma$ -bond of amorphous carbon films to give repulsion force, contributing low friction. However, no one knows what will happen if the H and F doped amorphous carbon (a-C:H and a-C:H:F) films are taken to slide on each other. The work aims to study the tribological properties of a-C:H sliding on a-C:H:F film and explore the mechanism of tribology between the a-C:H and a-C:H:F films with the variation of loads. a-C:H:F film was prepared on Si substrate by

收稿日期: 2023-03-18; 修訂日期: 2024-02-02

Received: 2023-03-18; Revised: 2024-02-02

基金项目: 甘肃省重点研发计划国际合作专项 (20YF8WA006)

Fund: International Cooperation Project of Key R&D Program of Gansu Province (20YF8WA006)

引文格式: 唐诗琪, 邢朝阳, 王圆圆, 等. 异质 a-C:H/a-C:H:F 配副的摩擦学行为研究[J]. 表面技术, 2024, 53(7): 107-115.

TANG Shiqi, XING Zhaoyang, WANG Yuanyuan, et al. Tribological Properties of a-C:H Sliding on a-C:H:F Films[J]. Surface Technology, 2024, 53(7): 107-115.

\*通信作者 (Corresponding author)

plasma enhanced chemical vapor deposition and a-C:H film was deposited with magnetron sputtering of a carbon target in methane and argon atmosphere, respectively. Then, the tribology behaviors were evaluated on a commercial reciprocating ball-on-disk tribometer (CSM TRB 3 TRIBOMETER, Switzerland) with the test frequency and the total sliding times were 9 000 at 5 Hz, respectively. Normal load was set to 2, 4, 6, 8 and 10 N, respectively. Surface morphology of the a-C:H:F films were analyzed by SEM, and the mechanical properties were investigated by nanoindentation tests, with the depth no more than 1/10 of the a-C:H:F film thickness. The structure and tribology properties of the a-C:H:F films were tested by Raman spectroscopy, XPS spectroscopy and FTIR spectroscopy, respectively. Through this characterization results, it was found that the effect of fluorine doping played a key role in reducing friction coefficient as well as wear rate. The friction coefficient of a-C:H:F film decreased gradually and the curve was becoming stable with the increase of normal load, and the friction coefficients were 0.037, 0.027, 0.025, 0.021, and 0.018, respectively. While the wear rates of a-C:H:F film reduced with increase of the load from 2 to 10 N, which were  $1.991 \times 10^{-8}$ ,  $1.212 \times 10^{-8}$ ,  $0.881 \times 10^{-8}$ ,  $0.721 \times 10^{-8}$ ,  $0.557 \times 10^{-8} \text{ mm}^3/(\text{N}\cdot\text{m})$ , respectively. The low friction coefficient can be ascribed to the transformation of  $\text{sp}^3$  to  $\text{sp}^2$  structure and promote the increase of  $\text{sp}^2\text{-C}$  clusters in the film which can be proved by typical Raman spectrum. The low wear rate can be attributed to the wear debris, which prevent the direct contact of the a-C:H and a-C:H:F films. Fluorine also has effect of passivating film surface and electrostatic repulsion as hydrogen do. Generally, a-C:H:F films prepared by PECVD have a superior anti-friction and anti-wear ability to couple with a-C:H balls.

**KEY WORDS:** tribological properties; fluorine doping; amorphous carbon film; PECVD

非晶碳膜（a-C:H）具有良好的力学性能、化学惰性、生物相容性，以及较低的摩擦因数，在机械、模具等领域得到广泛应用，引起了研究者的关注<sup>[1-2]</sup>。其中，含氢碳薄膜具有更低的摩擦因数，受到广泛关注。模拟实验结果表明，由于氢的电负性较低，氢化表面带有正电荷，并产生了排斥力，从而减小了摩擦和磨损<sup>[3-4]</sup>。非晶态含氢碳（a-C:H）膜具有优良的摩擦学性能和力学性能，因此在高精度轴承、生物医学植入手体、硬盘等方面具有广泛的应用前景<sup>[5]</sup>。由于a-C:H薄膜对湿度较敏感，在高湿度下其摩擦因数急剧增大，因此成为研究热点<sup>[6-8]</sup>。使用S、Si、F、N、Ti、W等对a-C:H薄膜进行掺杂<sup>[9-10]</sup>是有效的改进方法<sup>[11-15]</sup>，近年来人们针对F掺杂的研究逐渐增多，F是电负性最大的元素，与H一样，它具有外层单电子，可以有效饱和a-C:H薄膜表面悬键，降低表面自由能，形成化学惰性表面<sup>[16-17]</sup>。同时，氟化表面带有负电，在与其他摩擦副对磨时会产生排斥力，减小摩擦界面剪切力，形成低剪切界面，从而降低摩擦因数。更重要的是，氟化碳薄膜的表面疏水性有助于在潮湿环境下达到优良的润滑性能<sup>[18]</sup>。

通过氟改性碳薄膜的方法主要有2种，即等离子体表面处理（表面氟化）、等离子增强化学气相沉积（PECVD）。前者的作用深度有限（约数十纳米），限制了其实际应用<sup>[19]</sup>。PECVD技术利用含氟气体作为前驱气体来制备含氟碳薄膜（a-C:H:F），并通过偏压、气体流量、占空比和时间等参数，调控a-C:H:F薄膜的组分和结构<sup>[20]</sup>。在PECVD过程中，因为碳的配位数为4，氟的配位数为1，F的掺入会减少碳-碳交联，从而降低薄膜的硬度、弹性恢复能力和耐磨性<sup>[21]</sup>，

如何在获得超低摩擦因数的同时，使氟化碳膜兼备较低的磨损率成为亟待解决的问题<sup>[22]</sup>。

针对上述问题，文中提出异质配副降低摩擦磨损的新方法。采用PECVD方法，在不同气流和工艺下沉积a-C:H:F薄膜，与商用a-C:H薄膜配副，研究它在相对湿度为(40±5)%的空气中的摩擦学性能，拟为a-C:H:F薄膜在实际领域的应用提供一定理论和技术支持。

## 1 试验

### 1.1 样品制备

采用PECVD技术制备a-C:H:F薄膜。a-C:H:F薄膜的制备过程可以分为以下3步：清洗，采用Ar等离子体对基底进行清洗，将Ar气流速控制在0.15 L/min，偏压为1 000 V，气体压力为19 Pa，电流为0.8 A，占空比为80.1%，频率为78.9 kHz，清洗时间为30 min；过渡层制备，Ar 0.05 L/min，CH<sub>4</sub> 0.02 L/min，偏压为650 V，气体压力为26 Pa，电流为0.22 A，占空比为80.1%，频率为79.4 kHz，时间为1 h，制备过渡层可以让薄膜与基底结合更加紧密；a-C:H:F薄膜沉积，Ar 0.015 L/min，CH<sub>4</sub> 0.02 L/min，CF<sub>4</sub> 0.050 L/min，偏压为650 V，压力为25 Pa，电流为0.2 A，占空比为80.1%，频率为79.4 kHz，时间为1.5 h。a-C:H薄膜购自上海新弧源涂层技术有限公司。

### 1.2 结构及性能表征

利用场发射扫描电子显微镜（FESEM，JSM-6071F，Japan）研究薄膜的厚度和断面形貌。利用

X 射线光电子能谱 (XPS, ESCALAB 250Xi, USA) 分析 a-C:H:F 薄膜的结构、化学键和组成。利用显微共焦拉曼光谱仪 (Raman, LabRAM HR Evolution, HORIBA Jobin Yvon, France) 检测了摩擦前后 a-C:H:F 薄膜的键合信息, 激发波长为 532 nm。采用 IFS 66v/S 型傅里叶 FTIR 光谱仪 (FTIR, Bruker, France) 对薄膜表面官能团进行定性分析。借助原位纳米力学试验机 (Ti-950, Hysitron, USA) 测量 a-C:H:F 薄膜的硬度、弹性模量。

在相对湿度为(40±5)%的空气中, 使用往复模式 CSM TRB 3 摩擦机 (Tribometer 3, Switzerland) 研究 a-C:H:F 薄膜的摩擦学特性。采用 a-C:H 薄膜作为摩擦配副, 其直径为 6.0 mm。试验频率和滑动总次数分别为 5 Hz 和 9 000 次, 外加载荷分别为 2、4、6、8、10 N。

## 2 结果及分析

制备的 a-C:H:F 薄膜的 FE-SEM 断面照片如图 1 所示, 可见薄膜的结构均匀致密, 与基底的结合状态良好, 厚度约为 595 nm。纳米压痕测量结果表明, 薄膜的弹性恢复系数为 85%, 硬度和弹性模量分别为 14.19、68.10 GPa, 表明薄膜具有高硬度、低弹性模量、高弹性恢复率等力学性能。a-C:H:F 薄膜的显微共焦 Raman 光谱图及其对应的高斯函数拟合结果如图 2 所示。与 a-C:H 薄膜的 Raman 光谱一样, a-C:H:F 薄膜在 1 000~2 000 cm<sup>-1</sup> 范围内具有一个较宽且不对称的 Raman 光谱。通过高斯拟合, 将上述宽峰拟合为 2 个以 1 345、1 534 cm<sup>-1</sup> 为中心的 D 峰和 G 峰, 说明 a-C:H:F 薄膜在掺杂后同样具有典型的非晶碳基网络交联结构<sup>[23]</sup>。另外, 对偶球的显微共焦 Raman 光谱图及三维表面形貌如图 3 所示, 薄膜的 D 峰与 G 峰的面积比 ( $I_D/I_G$ ) 为 2.34, 经三维测算 a-C:H 薄膜对偶球的表面粗糙度为 6.63 μm。

a-C:H:F 薄膜的高斯拟合参数如表 1 所示, a-C:H:F 薄膜的 D 峰和 G 峰面积分别为 39 914.235、47 800.719。a-C:H:F 薄膜的 D 峰半高宽 ( $H_{FWHM\ D}$ ) 和 G 峰半高宽 ( $H_{FWHM\ G}$ ) 分别为 326.126、183.090。

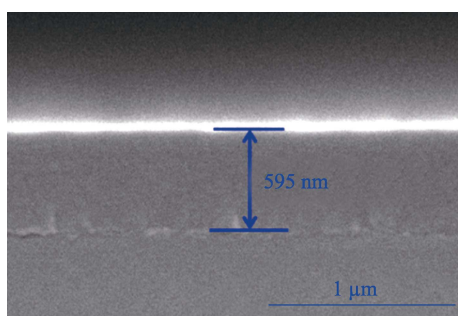


图 1 a-C:H:F 薄膜断面扫描电镜图像  
Fig.1 SEM image of a-C:H:F film

一般情况下, D 峰通常与碳基网络结构的无序度相关, D 峰的拓宽意味着薄膜无序度的增加、 $sp^2$  团簇的增大<sup>[24]</sup>, 说明 F 元素的掺杂一方面促进了薄膜中  $sp^2$ -C 的杂化, 另一方面增大了薄膜的无序度。

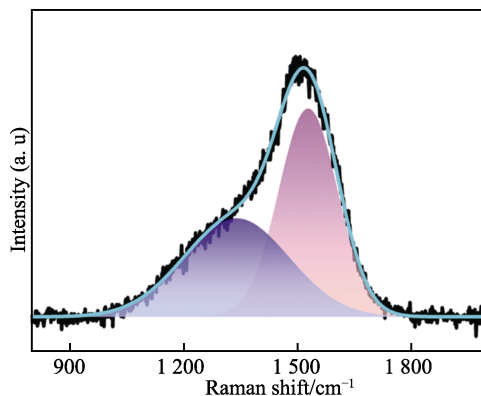


图 2 a-C:H:F 薄膜的 Raman 光谱高斯拟合图  
Fig.2 Gaussian fitting Raman spectrum of the a-C:H:F film

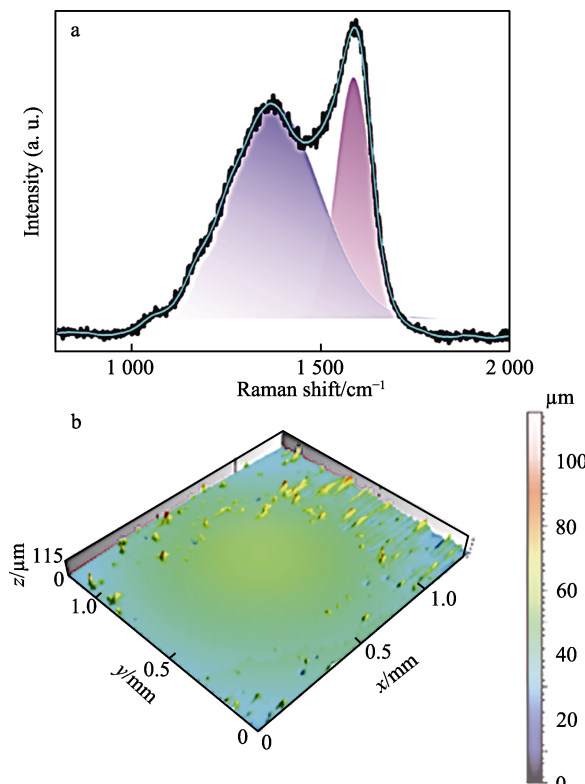


图 3 a-C:H 薄膜对偶球的 Raman 光谱高斯拟合  
图 (a) 和三维表面形貌 (b)

Fig.3 Gaussian fitting Raman spectrum (a) and 3D surface morphology (b) of the a-C:H film coupled ball

表 1 a-C:H:F 薄膜的 Raman 高斯拟合峰值信息  
Tab.1 Gaussian fitting Raman spectrum information of the a-C:H:F film

Parameters	D peak	G Peak	$I_D/I_G$
Peak Num/cm <sup>-1</sup>	1 345	1 534	
Peak Area	39 914.235	47 800.719	0.835
FWHM	326.126	183.090	

a-C:H:F 薄膜的 XPS C 1s 光谱如图 4 所示。通过高斯拟合，将 C 1s 峰拟合为以下 6 个高斯峰，分别位于 284.4、285.1、286.1、286.6、(288±0.2)、289.2 eV，该 6 个拟合峰分别对应 C=C、C—C、C—O、C—CF、C—F/C=O、C—F<sub>2</sub> 基团。其中，C=C 键合和 C—C 键合由非晶碳薄膜中 sp<sup>2</sup> 和 sp<sup>3</sup> 键杂化构型贡献，联合组成非晶碳的网络交联构型。C—O 键合和 C=O 键合可能由 a-C:H:F 薄膜暴露在空气中时其表面所沾染的污染物所致，C—CF、C—F、C—F<sub>2</sub> 基团的出现则归因于沉积过程中 F 元素的掺杂。

a-C:H:F 薄膜的 FTIR 光谱如图 5 所示。从图 5 可以看出，a-C:H:F 薄膜表现出 6 个显著的振动峰，位于 2 850 cm<sup>-1</sup> 和 2 920 cm<sup>-1</sup> 处的 2 个强峰分别归属于 sp<sup>3</sup> CH<sub>2</sub> 的对称及反对称伸缩振动峰；3 300 cm<sup>-1</sup>

处的峰为 sp<sup>1</sup> CH 的伸缩振动峰；位于 1 240~1 466 cm<sup>-1</sup> 的吸收峰为 CF<sub>x</sub> (x=1, 2, 3) 键的伸缩振动峰；位于 1 630 cm<sup>-1</sup> 的吸收峰为氟化烯烃峰 (HFC=) 或氟化芳香环 (H<sub>2</sub>C=) 的振动模式峰。另外，位于 1 720 cm<sup>-1</sup> 处的吸收峰归因于 F<sub>2</sub>C= 的基团振动；HFC=、F<sub>2</sub>C= 峰由 C=C 的伸缩振动形成，且向更高频率移动，以部分或者完全氟化的状态存在。

a-C:H 薄膜对偶球与 a-C:H:F 薄膜在大气环境下不同载荷时的摩擦因数曲线如图 6a 所示。a-C:H:F 薄膜在不同载荷下的平均摩擦因数分别为 0.037、0.027、0.025、0.021、0.018。从图 6a 中可以看出，a-C:H:F 薄膜除了在载荷 2 N 下的摩擦因数曲线在后半段出现上升趋势外，在其他载荷下其摩擦因数曲线都较平稳。

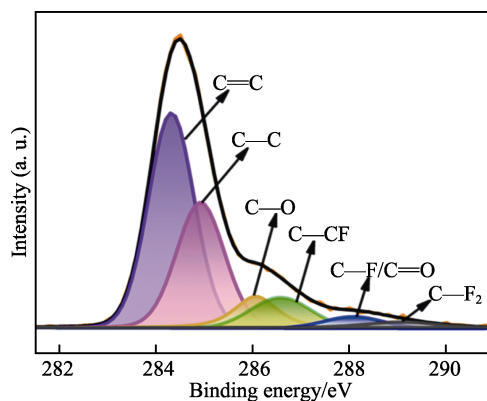


图 4 a-C:H:F 薄膜的 XPS C 1s 拟合图谱  
Fig.4 XPS C 1s fitting spectrum of the a-C:H:F film

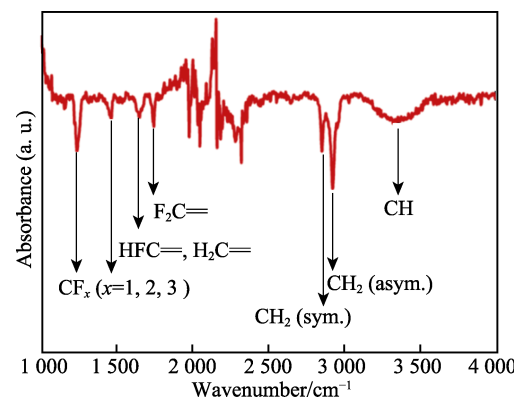


图 5 a-C:H:F 薄膜的红外光谱  
Fig.5 FTIR spectra of the a-C:H:F film

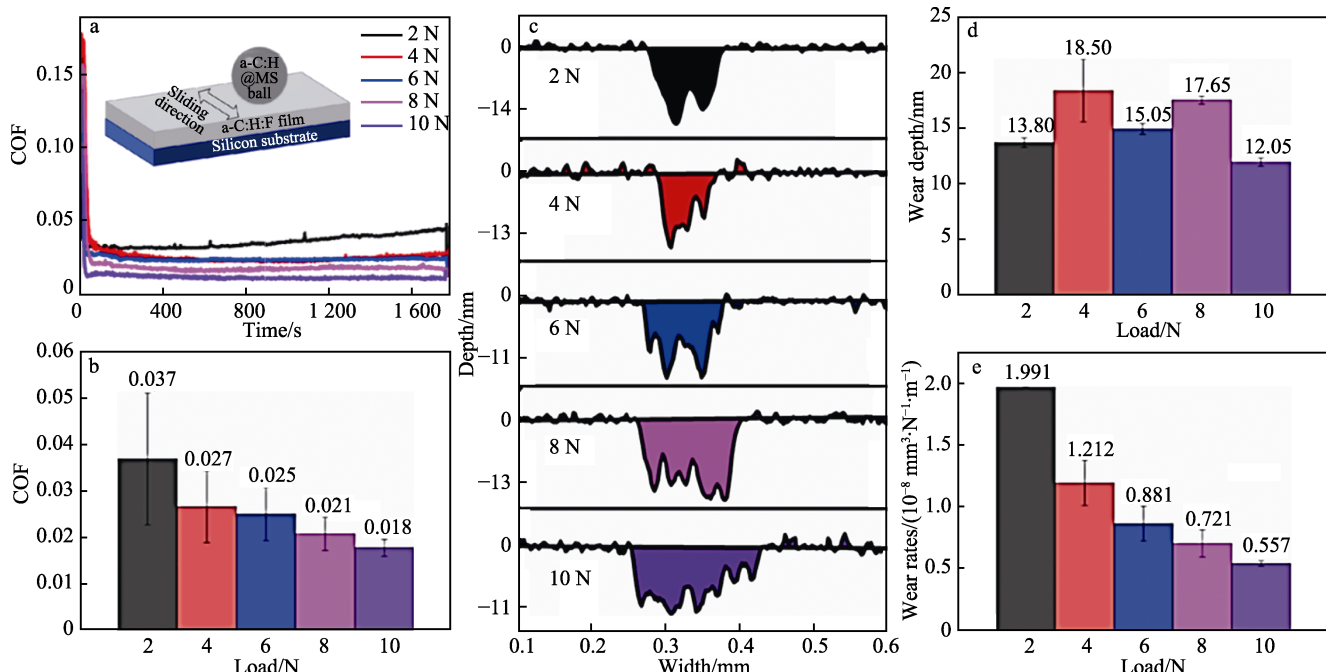


图 6 a-C:H:F 薄膜的摩擦因数曲线 (a)、摩擦因数柱状图 (b)、磨损深度曲线 (c)、磨损深度柱状图 (d) 及磨损率 (e)  
Fig.6 Friction coefficient curves (a), histogram statistics of the friction coefficient (b), wear depth curves (c), histogram statistics of the wear depths (d) and wear rates (e) of the a-C:H:F film

从柱状数据图(图 6b)中可以清楚看出, a-C:H:F 薄膜的摩擦因数随着附加载荷的不断增大而降低。诸多研究表明, 含氢 DLC 薄膜通常在较高载荷下具有更低的摩擦因数<sup>[25-27]</sup>, 干摩擦的摩擦因数用式(1)表示。

$$\mu = \frac{F_f}{F_n} = k\pi \left( \frac{3R}{4E} \right)^{\frac{2}{3}} \tau F_n^{-\frac{1}{3}} \quad (1)$$

式中:  $F_f$  为摩擦力;  $F_n$  为载荷;  $\tau$  为剪切压力。

在 DLC 表面加载时, 剪切力  $\tau$  一般保持不变, 载荷与摩擦因数呈负相关。此外, 有研究证明, DLC 薄膜转移层的形成程度随着滑动速度和载荷的增加而增加<sup>[28]</sup>, 高度无序的类石墨覆盖区和低剪切区域的形成, 使得 DLC 的稳态摩擦因数随着载荷的增加而减少。

a-C:H:F 薄膜在摩擦过程中摩擦因数降低的原因是 F 元素的引入, F 在钝化薄膜表面存在静电排斥作用。在 a-C:H:F 薄膜中, F 是电负性最大的元素, F 原子与 C 原子之间的电负性差值较大, 当 a-C:H:F 薄膜中 C 原子与 F 原子成键时, C 原子的部分电荷向 F 原子转移, 使得 a-C:H:F 薄膜表面 F 原子带有更多的负电荷, 造成薄膜表面之间存在静电排斥作用, 因此 a-C:H:F 薄膜呈现出更低的摩擦因数<sup>[25]</sup>。同时, 薄膜在相对湿度为(40±5)%的潮湿环境中保持着较低的摩擦因数, 是因 CFX 基团的疏水性带来的氟化碳薄膜表面疏水性, 有助于它在潮湿环境下表现出优良的润滑性能, 使 a-C:H:F 薄膜在大气环境下也具有较低的摩擦因数和磨损率。

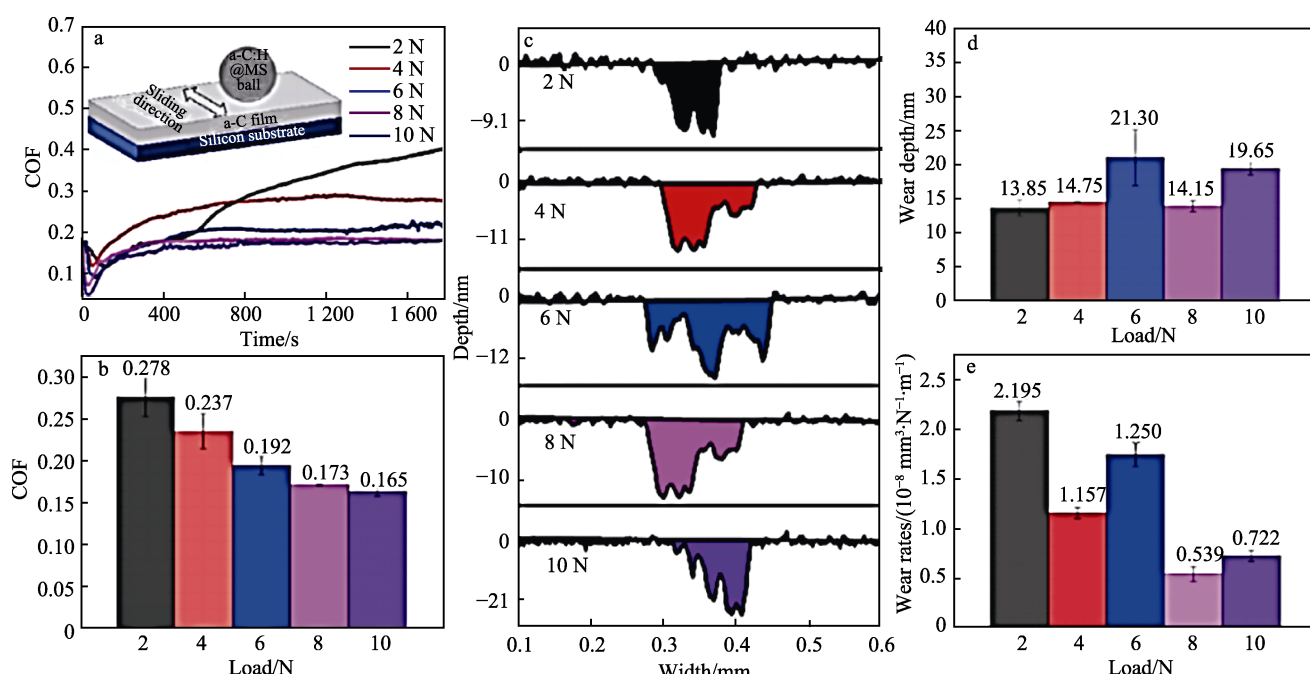


图 7 a-C 薄膜的摩擦因数曲线(a)、摩擦因数柱状图(b)、磨损深度曲线(c)、磨损深度柱状图(d)及磨损率(e)

Fig.7 Friction coefficient curves (a), histogram statistics of the friction coefficient (b), wear depth curves (c), histogram statistics of the wear depths (d) and wear rates (e) of the a-C film

在摩擦试验结束后, 采用非接触三维轮廓仪(MicroXAM-800, KLA-Tencor, USA)评估薄膜上磨损痕迹的磨损量。a-C:H:F 薄膜在不同法向载荷下的磨损深度 2D 曲线如图 6c 所示, 其磨损深度如图 6d 所示。可以看出, a-C:H:F 薄膜在不同附加载荷下的磨损深度在 12.05~18.50 nm 之间。另外, a-C:H:F 薄膜的磨损率如图 5e 所示, 在不同附加载荷下 a-C:H:F 薄膜的磨损率分别为  $1.991 \times 10^{-8}$ 、 $1.212 \times 10^{-8}$ 、 $0.881 \times 10^{-8}$ 、 $0.721 \times 10^{-8}$ 、 $0.557 \times 10^{-8} \text{ mm}^3/(\text{N}\cdot\text{m})$ 。在摩擦因数方面, a-C:H:F 薄膜与相同配副 a-C:H 薄膜对偶球摩擦时, 具有比 a-C 薄膜和 a-C:H 薄膜配副更低的摩擦因数, 且 F 元素掺杂 a-C:H 薄膜有助于降低薄膜的磨损率, 如图 7、图 8 所示。

为了进一步证实上述结论, 对不同载荷摩擦实验后的薄膜表面磨痕进行了 Raman 分析, 结果如图 9a 所示。a-C:H:F 薄膜表面磨痕平整且痕迹很浅, a-C:H:F 薄膜表面磨痕在 1 000~2 000 cm<sup>-1</sup> 范围内的 Raman 峰被拟合为 2 个高斯峰, 结果统计于表 2 中。在不同载荷下, 磨痕的  $I_D/I_G$  如图 9b 所示, 可以看出, a-C:H:F 薄膜的  $I_D/I_G$  随着载荷的增加, 从 0.764 升至 1.384。这一变化趋势与摩擦因数的变化趋势相反,  $I_D/I_G$  的增大表示磨痕结构中  $\text{sp}^2\text{-C}/\text{sp}^3\text{-C}$  的比值增大<sup>[23,29]</sup>, 高于 0.7 表明磨痕组织成分中石墨化程度很高, 这种类石墨结构的形成证明在摩擦过程中诱导了  $\text{sp}^3$  向  $\text{sp}^2$  结构的转化, 促进了薄膜中  $\text{sp}^2$ -C 团簇的增加, 达到了降低摩擦因数的目的。摩擦过程及其相关机理如图 10 所示。

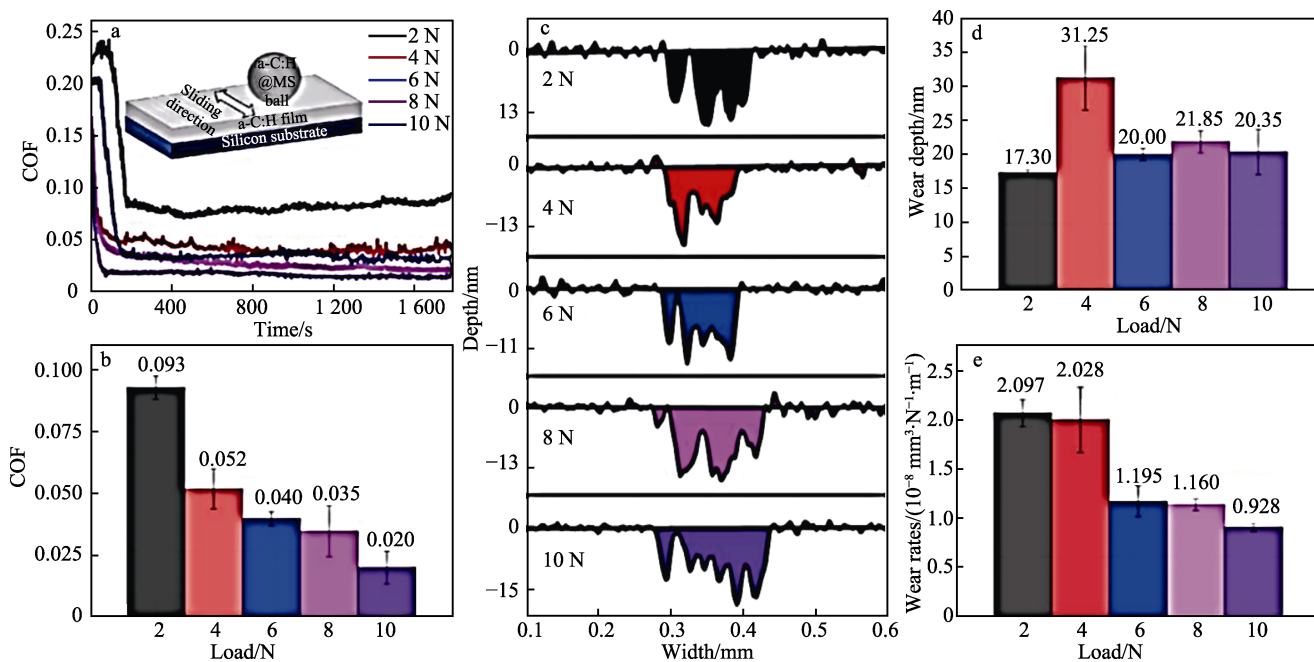


图8 a-C:H 薄膜的摩擦因数曲线 (a)、摩擦因数柱状图 (b)、磨损深度曲线 (c)、  
磨损深度柱状图 (d) 及磨损率 (e)

Fig.8 Friction coefficient curves (a), histogram statistics of the friction coefficient (b), wear depth curves (c), histogram statistics of the wear depths (d) and wear rates (e) of the a-C:H film

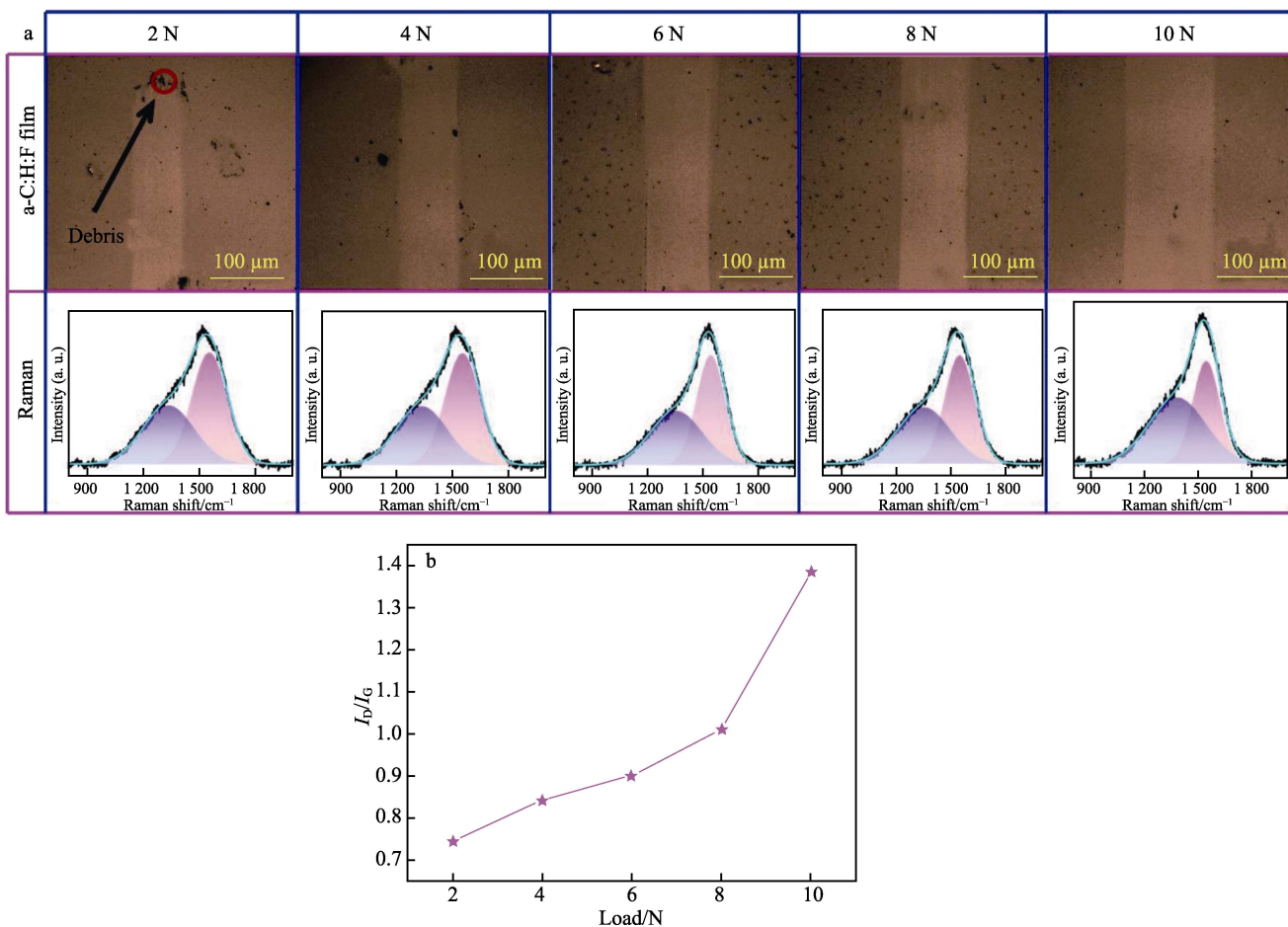


图9 不同附加载荷下 a-C:H:F 薄膜磨痕图像、磨痕 Raman 拟合图 (a) 及  $I_D/I_G$  变化曲线 (b)  
Fig.9 Image and Raman fitting spectra (a) and  $I_D/I_G$  values curve (b) of the a-C:H:F wear  
debris under the different applied loads

表 2 a-C:H:F 薄膜表面磨痕处的 Raman 拟合结果  
Tab.2 Raman fitting results of debris position of the a-C:H:F film

Debris position on different loads/N	Parameters	D	G	$I_D/I_G$
2	Peak Num/cm <sup>-1</sup>	1 332	1 553	
	Peak Area	144 102.706	188 626.173	0.764
	FWHM	325.774	223.960	
4	Peak Num/cm <sup>-1</sup>	1 346	1 544	
	Peak Area	89 784.025	106 512.673	0.843
	FWHM	328.156	191.669	
6	Peak Num/cm <sup>-1</sup>	1 354	1 542	
	Peak Area	74 173.280	82 212.458	0.902
	FWHM	334.634	183.898	
8	Peak Num/cm <sup>-1</sup>	1 350	1 547	
	Peak Area	89 887.808	88 821.945	1.012
	FWHM	336.644	193.734	
10	Peak Num/cm <sup>-1</sup>	1 380	1 544	
	Peak Area	117 027.330	84 542.665	1.384
	FWHM	373.685	117.557	

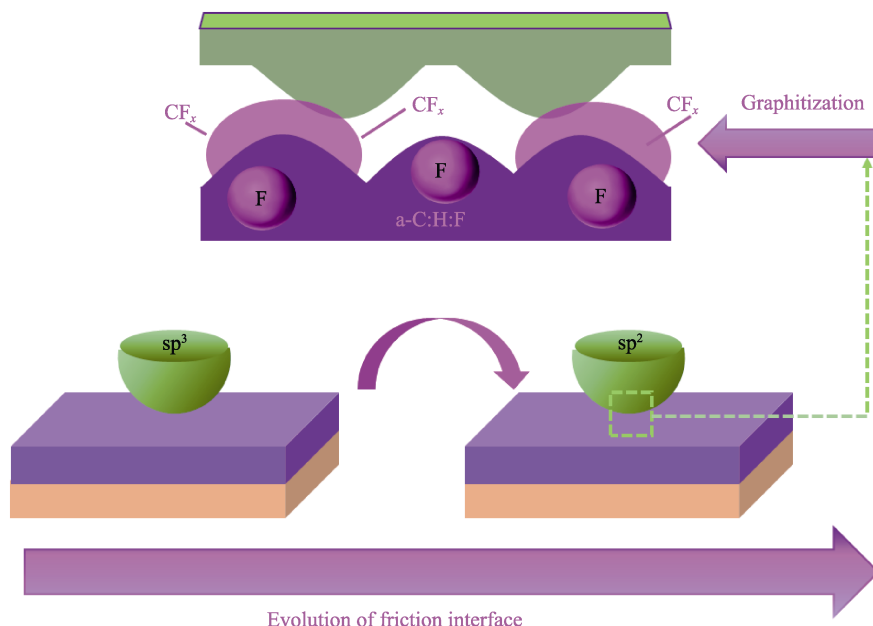


图 10 a-C:H:F 薄膜与 a-C:H 薄膜对偶球摩擦的机理  
Fig.10 Mechanism of dual friction process between a-C:H:F film and a-C:H

### 3 结论

采用 PECVD 法在 CH<sub>4</sub>、CF<sub>4</sub> 气氛中制备 a-C:H:F 薄膜, 该薄膜具有低摩擦因数、低磨损率, 以及优异的力学性能(高硬度、高弹性回复率), 符合 DLC 薄膜的固有性质。推测其优异的摩擦性能与含有的氟元素和薄膜结构相关, 通过系列不同附加载荷摩擦实验和分析检测后, 得出如下结论。

1) a-C:H:F 薄膜在相对湿度为(40±5)%的环境中摩擦, 随着附加载荷的增加, a-C:H:F 薄膜与 a-C:H

薄膜对偶球的摩擦因数经过短时间跑合后逐渐降低, 且曲线较平稳。这是基于含氢碳膜本来的性质, 且磨合过程诱导了 sp<sup>3</sup> 向 sp<sup>2</sup> 结构的转化, 促进了薄膜中 sp<sup>2</sup>-C 团簇的增加。石墨化摩擦层的形成进一步降低了 a-C:H:F 薄膜的摩擦因数。

2) F 元素的掺杂一方面促进了薄膜中 sp<sup>2</sup>-C 杂化, 另一方面增加了薄膜的无序度。F 元素还具有钝化薄膜表面作用和静电排斥作用。这是由于氟化表面带有负电, 易与对偶面产生排斥力, 减小了摩擦界面剪切力, 形成了低剪切界面, 从而降低了摩擦体系的

摩擦因数。 $\text{CF}_x$  基团的疏水性带给氟化碳薄膜表面疏水性,有助于在潮湿环境下达到优良的润滑性能,使 a-C:H:F 薄膜在大气环境下也具有较低的摩擦因数和磨损率。

### 参考文献:

- [1] ROBERTSON J. Diamond-Like Amorphous Carbon[J]. Materials Science and Engineering: R: Reports, 2002, 37(4/5/6): 129-281.
- [2] CHARITIDIS C A. Nanomechanical and Nanotribological Properties of Carbon-Based Thin Films: A Review [J]. International Journal of Refractory Metals and Hard Materials, 2010, 28(1): 51-70.
- [3] ERDEMIR A. The Role of Hydrogen in Tribological Properties of Diamond-Like Carbon Films[J]. Surface and Coatings Technology, 2001, 146/147: 292-297.
- [4] DONNET C, FONTAINE J, GRILL A, et al. The Role of Hydrogen on the Friction Mechanism of Diamond-Like Carbon Films[J]. Tribology Letters, 2001, 9(3): 137-142.
- [5] ERDEMIR A, DONNET C. Tribology of Diamond-Like Carbon Films: Recent Progress and Future Prospects[J]. Journal of Physics D: Applied Physics, 2006, 39(18): R311-R327.
- [6] ERDEMIR A, NILUFER I B, ERYILMAZ O L, et al. Friction and Wear Performance of Diamond-Like Carbon Films Grown in Various Source Gas Plasmas[J]. Surface and Coatings Technology, 1999, 120/121: 589-593.
- [7] FONTAINE J, DONNET C, GRILL A, et al. Tribochemistry between Hydrogen and Diamond-Like Carbon Films[J]. Surface and Coatings Technology, 2001, 146/147: 286-291.
- [8] KIM H I, LINCE J R, ERYILMAZ O L, et al. Environmental Effects on the Friction of Hydrogenated DLC Films[J]. Tribology Letters, 2006, 21(1): 51-56.
- [9] 郭培林, 贾倩, 孟树文, 等. 元素掺杂对类金刚石薄膜摩擦学性能的影响[J]. 中国表面工程, 2021, 34(4): 19-29.
- [10] 张斌, 吉利, 鲁志斌, 等. 工程导向固体超滑(超低摩擦)研究进展[J]. 摩擦学学报, 2023, 43(1): 3-17.
- ZHANG B, JI L, LU Z B, et al. Progress on Engineering Oriented Solid Superlubricity[J]. Tribology, 2023, 43(1): 3-17.
- [11] SÁNCHEZ-LÓPEZ J C, BELIN M, DONNET C, et al. Friction Mechanisms of Amorphous Carbon Nitride Films under Variable Environments: A Triboscopic Study[J]. Surface and Coatings Technology, 2002, 160(2/3): 138-144.
- [12] WANG F, WANG L P, XUE Q J. Fluorine and Sulfur Co-Doped Amorphous Carbon Films to Achieve Ultra-Low Friction under High Vacuum[J]. Carbon, 2016, 96: 411-420.
- [13] ZHANG R H, PU J B, YANG Y C, et al. Probing the Frictional Properties of Sulfur-Doped Diamond-Like Carbon Films under High Vacuum by First-Principles Calculations[J]. Applied Surface Science, 2019, 481: 1483-1489.
- [14] JIANG J L, HAO J Y, WANG P, et al. Superlow Friction of Titanium/Silicon Codoped Hydrogenated Amorphous Carbon Film in the Ambient Air[J]. Journal of Applied Physics, 2010, 108(3): 448.
- [15] CHEN X C, KATO T, KAWAGUCHI M, et al. Structural and Environmental Dependence of Superlow Friction in Ion Vapour-Deposited A-C:H:Si Films for Solid Lubrication Application[J]. Journal of Physics D: Applied Physics, 2013, 46(25): 255304.
- [16] MEMMING R. Properties of Polymeric Layers of Amorphous Hydrogenated Carbon Produced by a Plasma-Activated Chemical Vapour Deposition Process I: Spectroscopic Investigations[J]. Thin Solid Films, 1986, 143(3): 279-289.
- [17] YU G Q, TAY B K, SUN Z, et al. Properties of Fluorinated Amorphous Diamond Like Carbon Films by PECVD[J]. Applied Surface Science, 2003, 219(3/4): 228-237.
- [18] BUTTER R S, WATERMAN D R, LETTINGTON A H, et al. Production and Wetting Properties of Fluorinated Diamond-Like Carbon Coatings[J]. Thin Solid Films, 1997, 311(1/2): 107-113.
- [19] YU G Q, TAY B K, SUN Z. Fluorinated Amorphous Diamond-Like Carbon Films Deposited by Plasma-Enhanced Chemical Vapor Deposition[J]. Surface and Coatings Technology, 2005, 191(2/3): 236-241.
- [20] DAGOSTINO R, LAMENDOLA R, FAVIA P, et al. Fluorinated Diamondlike Carbon Films Deposited from Radio-Frequency Glow Discharge in a Triode Reactor[J]. Journal of Vacuum Science Technology A: Vacuum Surfaces and Films, 1994, 12(2): 308-313.
- [21] HATADA R, BABA K. Preparation of Hydrophobic Diamond Like Carbon Films by Plasma Source Ion Implantation[J]. Nuclear Instruments and Methods in Physics Research Section B: Beam Interactions with Materials and Atoms, 1999, 148(1/2/3/4): 655-658.
- [22] WEI L, ZHANG B, ZHOU Y, et al. Ultra-Low Friction of Fluorine-Doped Hydrogenated Carbon Film with Curved Graphitic Structure[J]. Surface and Interface Analysis, 2013, 45(8): 1233-1237.
- [23] FERRARI A C, ROBERTSON J. Interpretation of Raman Spectra of Disordered and Amorphous Carbon[J]. Physical Review B, 2000, 61(20): 14095-14107.
- [24] DILLON R O, WOOLLAM J A. 148. Use of Raman Scattering to Investigate Disorder and Crystallite Formation in AS-Deposited and Annealed Carbon Films[J].

- Carbon, 1984, 22(2): 220.
- [25] YU Q, CHEN X C, ZHANG C H, et al. Influence Factors on Mechanisms of Superlubricity in DLC Films: A Review [J]. Frontiers in Mechanical Engineering-Switzerland, 2020, 6: 65.
- [26] ZHANG S L, WAGNER G, MEDYANIK S N, et al. Experimental and Molecular Dynamics Simulation Studies of Friction Behavior of Hydrogenated Carbon Films [J]. Surface and Coatings Technology, 2004, 177/178: 818-823.
- [27] LIU Y H, WANG L, LIU T Y, et al. Effect of Normal Loads and Mating Pairs on the Tribological Properties of Diamond-Like Carbon Film[J]. Wear, 2021, 486/487: 204083.
- [28] KIM D W, KIM K W. Effects of Sliding Velocity and Normal Load on Friction and Wear Characteristics of Multi-Layered Diamond-Like Carbon (DLC) Coating Prepared by Reactive Sputtering[J]. Wear, 2013, 297(1/2): 722-730.
- [29] YU Q, CHEN X C, ZHANG C H, et al. Influencing Mechanisms of Deposition Bias Voltage on Superlubricious A-C: H Films: Key Role of Nanoclustering Structures in Controlling Structural Evolution of Transfer Film[J]. Carbon, 2022, 196: 499-509.

(上接第 84 页)

- [23] MICALLEF C, ZHUK Y, ARIA A I. Surface Finishing and Tool Wear in Single Point Diamond Turning of Chemical Vapour Deposited Tungsten Carbide Hard Coatings [J]. Surface and Coatings Technology, 2022, 447: 128864.
- [24] DOMITNER J, SILVAYEH Z, BUZOLIN R H, et al. Microstructure Characterization of Nickel Matrix Composite Reinforced with Tungsten Carbide Particles and Produced by Laser Cladding[J]. Advanced Engineering Materials, 2022, 24(11): 2200463.
- [25] TESTA V, MORELLI S, BOLELLI G, et al. Corrosion and Wear Performances of Alternative TiC-Based Thermal Spray Coatings[J]. Surface and Coatings Technology, 2022, 438: 128400.
- [26] ZHANG Y P, WANG Q, RAMACHANDRAN C S, et al. Microstructure and Performance of High-Velocity Oxygen-Fuel Coupled Physical Vapor Deposition (HVOF-PVD) Duplex Protective Coatings: A Review[J]. Coatings, 2022, 12(10): 1395
- [27] HAO E K, ZHAO X Q, AN Y L, et al. WC-Co Reinforced NiCoCrAlYTa Composite Coating: Effect of the Proportion on Microstructure and Tribological Properties[J]. International Journal of Refractory Metals and Hard Materials, 2019, 84: 104978.
- [28] GATES R S, HSU M, KLAUS E E. Tribocorrosion Mechanism of Alumina with Water[J]. Tribology Transactions, 1989, 32(3): 357-363.
- [29] FISCHER T E, MULLINS W M. Chemical Aspects of Ceramic Tribology[J]. The Journal of Physical Chemistry, 1992, 96(14): 5690-5701.
- [30] 刘宁, 王建章, 陈贝贝, 等. 氧化铝陶瓷在海水润滑下的摩擦学行为研究[J]. 润滑与密封, 2013, 38(5): 55-59.
- [31] LIU N, WANG J Z, CHEN B B, et al. Tribological Behavior of Alumina Ceramic under Lubrication of Seawater[J]. Lubrication Engineering, 2013, 38(5): 55-59.
- [32] 王丁丁, 马贤, 王筠, 等. 利用拉曼光谱鉴定碳化钨涂层材料的物相结构[J]. 稀有金属与硬质合金, 2022, 50(1): 37-41.
- [33] WANG D D, MA X, WANG J, et al. Identification of Phase Composition of Tungsten Carbide Coating Materials by Raman Spectrum[J]. Rare Metals and Cemented Carbides, 2022, 50(1): 37-41.
- [34] ELMRABET S, ABAD M D, LÓPEZ-CARTES C, et al. Thermal Evolution of WC/C Nanostructured Coatings by Raman and in Situ XRD Analysis[J]. Plasma Processes and Polymers, 2009, 6(Sup.1): 444-449.
- [35] PENG F, YU W W, LU Y, et al. Enhancement of Low-Temperature Gas-Sensing Performance Using Substoichiometric  $\text{WO}_{3-x}$  Modified with CuO[J]. ACS Applied Materials & Interfaces, 2020, 12(37): 41230-41238.
- [36] LORITE I, ROMERO J J, FERNÁNDEZ J F. Effects of the Agglomeration State on the Raman Properties of  $\text{Co}_3\text{O}_4$  Nanoparticles[J]. Journal of Raman Spectroscopy, 2012, 43(10): 1443-1448.